Frontiers in Bioscience Landmark

Front. Biosci. (Landmark Ed) **2023**; 28(5): 100
https://doi.org/10.31083/j.fbl2805100

Original Research

Rhein Inhibited Ferroptosis and EMT to Attenuate Diabetic Nephropathy by Regulating the Rac1/NOX1/β-Catenin Axis

Dan Xiong[1,†], Wei Hu[2,*,†], Xiaofang Han[3], Yahong Cai[4]

[1]Department of Nephrology, The First Hospital of Hunan University of Chinese Medicine, 410021 Changsha, Hunan, China
[2]Department of Endocrinology, The First Hospital of Hunan University of Chinese Medicine, 410021 Changsha, Hunan, China
[3]Department of Infectious Diseases, The First Hospital of Lanzhou University, 730099 Lanzhou, Gansu, China
[4]Department of Chronic Disease Management, The First Hospital of Hunan University of Chinese Medicine, 410021 Changsha, Hunan, China
*Correspondence: hu13874983405@163.com (Wei Hu)
[†]These authors contributed equally.

Academic Editor: Paramjit S. Tappia
Submitted: 8 November 2022 Revised: 6 January 2023 Accepted: 11 January 2023 Published: 25 May 2023

Abstract

Background: Diabetic nephropathy (DN) is one of the most serious complications of diabetes. Rhein has been reported to be effective in treating DN. This study aimed to investigate the role and mechanism of rhein in the treatment of DN. **Methods**: High glucose-induced (HG) podocyte injury model and streptozocin-induced (STZ) DN mouse model were constructed and intervened with rhein. Cell viability was detected by Cell Counting Kit-8 (CCK-8) assay. The reactive oxygen species (ROS) level was measured by flow cytometry. The expression of Ras-related C3 botulinum toxin substrate 1 (Rac1), NADPH Oxidase 1 (NOX1), and β-catenin were measured by quantitative real-time PCR (RT-qPCR). The contents of glutathione peroxidase 4 (GPX4), α-smooth muscle actin (α-SMA), Nephrin, and Podocin were characterized by immunofluorescence (IF) staining. Hematoxylin-eosin (HE) staining and Masson staining were employed to observe the renal morphological changes and tubulointerstitial fibrosis. The contents of α-SMA and Nephrin were detected by immunohistochemistry (IHC) staining. The kits were utilized to analyze various biochemical indicators. **Results**: Rhein inhibited the HG-induced accumulation of ROS, malondialdehyde (MDA), and Fe^{2+}, and the expression of α-SMA, Transferrin Receptor 1 (TFR1), acyl-CoA synthetase long-chain family member 4 (ACSL4), Vimentin, Snail, and Desmin. Rhein inhibited the expression of Rac1 and its downstream targets NOX1 and β-catenin. Rac1 silencing (si-Rac1) inhibited the accumulation of MDA and Fe^{2+} and the expression of Rac1, NOX1, β-catenin, α-SMA, TFR1, and ACSL4. Rac1 overexpression (oe-Rac1) resulted in the inhibition of superoxide dismutase (SOD), glutathione (GSH), GPX4 synthesis, and down-regulation of Recombinant Solute Carrier Family 7, Member 11 (SLC7A11) and Nephrin expression in HG-treated podocytes. Rac1 Lentivirus (LV-Rac1) injection significantly promoted the accumulation of MDA and Fe^{2+} and increased the expression of RAC1, NOX1, β-catenin, TFR1, ACSL4, and α-SMA in DN mice. **Conclusions**: Rhein inhibited ferroptosis and epithelial-mesenchymal transition (EMT) to attenuate DN by regulating the Rac1/NOX1/β-catenin axis.

Keywords: rhein; ferroptosis; EMT; DN; Rac1/NOX1/β-catenin axis

1. Introduction

Diabetic nephropathy (DN) is considered to be the main cause of end-stage renal disease, which is prone to high morbidity and mortality. The typical manifestation of DN is proteinuria, and other features include thickened glomerular basement membrane (GBM) and renal tubulointerstitial fibrosis [1,2]. Podocyte injury is considered to be the core link to cause proteinuria in the early stage of DN [3]. Podocytes are highly differentiated cells attached to the lateral side of the GBM and play an important role in maintaining renal functions [4]. Studies have shown that ferroptosis is involved in DN progression both *in vivo* and *in vitro* [5,6]. Ferroptosis is a programmed cell death mode that depends on reactive oxygen species (ROS) and iron [7]. Previous studies have suggested that the accumulation of iron and lipid peroxides may increase renal injury in DN by increasing oxidative stress [8]. In addition, epithelial-mesenchymal transition (EMT) in podocytes is also closely related to DN progression. EMT of Podocytes has been reported to cause renal tubulointerstitial fibrosis in DN [9,10]. Besides, EMT of podocytes has also been associated with the excretion of urinary albumin in DN [11]. At present, antihypertensive and hypoglycemic drugs are mainly applied to treat DN clinically, while drugs targeting the pathogenesis of DN are various but suffer from poor efficacy and safety [12]. For this situation, Chinese herbs and their extracts provide more options for the clinical treatment of DN [13].

Rhein, an anthraquinone compound isolated from Chinese herbal medicine such as *Rheum palmatum* L, *cassia* seed, *polygonum multiflorum*, *aloe*, and *polygonum cuspidatum* mainly by the ultrasonic nebulization extraction [14] and the microwave-assisted extraction [15]. It has been widely used for the treatment of various diseases with pharmacological properties including antibacterial, anti-inflammatory, kidney preserving, and antifibrosis [16]. Studies have found that rhein is effective in the

treatment of experimental DN, and its mode of action is the comprehensive result of multiple targets and multiple pathways [17–19]. Rhein can improve renal lesions and dyslipidemia in db/db DN mice [20]. Clinical studies have shown that the levels of total cholesterol, triglycerides, and transforming growth factor beta1 (TGF-β1) in glomerular mesangial cells are markedly reduced in DN patients after 4 and 6 months of oral rhein supplements [21]. In the further study of the mechanism of rhein on DN, it was found that rhein could inhibit the apoptosis and EMT of renal tubular epithelial cells and produce the antifibrotic effect, thus preventing the progressive development of DN [22]. However, the specific mechanism of rhein on DN remains to be clarified, which is one of the main causes limiting rhein to clinical application.

Ras-related C3 botulinum toxin substrate 1 (Rac1) is a member of the Rho family of small G proteins. Rac1 hyperactivation in glomerular podocytes is associated with the pathogenesis of familial proteinuria nephropathy [23]. Studies have shown that Rac1 deficiency can ameliorate podocyte injury and urinary albumin induced by streptozocin (STZ) in DN mice [24]. In addition, the Rac1/PAK1 signaling pathway promoted high glucose-induced EMT of podocytes *in vitro* by triggering β-catenin transcriptional activity [25]. NADPH oxidase 1 (NOX1) is a key factor in mediating ferroptosis [26]. In DN studies, inhibition of the NOX1/ROS/NF-κB pathway improved inflammation and extracellular matrix accumulation [27]. In addition, Rac1 regulated the production of NOX1-dependent ROS [28]. The wnt/β-catenin signaling pathway participates in rhein-ameliorating renal injury in DN mice [29]. These pieces of evidence suggest that the Rac1/Nox1/β-catenin axis may be involved in the development of DN. Studies have found that rhein could stably bind Rac1 by molecular docking [30,31]. However, it has not been investigated whether rhein inhibits the ferroptosis and EMT of podocytes to alleviate DN by regulating the Rac1/Nox1/β-catenin axis.

Therefore, this study explored the role and specific mechanism of rhein in the treatment of DN by constructing the podocyte high glucose (HG) model and mouse DN model and using rhein for intervention treatment, to provide new insights for the treatment of DN.

2. Materials and Methods

2.1 Cell Culture

The mouse glomerular podocyte (MPC5) (AW-CNM109, Abiowell, Changsha, China) was cultured in Dulbecco's modified Eagle's medium (DMEM) (D5796, Sigma, St. Louis, MO, USA) containing 10% fetal bovine serum (FBS) (10099141, Gibco, Waltham, MA, USA) and 1% Penicillin/Streptomycin (SV30010, Beyotime, Shanghai, China) and placed in a humidified incubator containing 5% CO_2 at 37 °C. When the cell confluence reached 70–80%, trypsin digestion, passage, and transfection experiments were carried out.

2.2 Construction of HG Injury Model and Intervention

In experiment 1, MPC5 was divided into 4 groups: normal glucose (NG), NG+Rhein, HG, and HG+Rhein. MPC5 was cultured in a serum-free medium for 12 h. MPC5 in the NG group was treated with 5.5 mM glucose and 24.5 mM mannitol for 48 h as control. MPC5 in the HG group was treated with 30 mM HG for 48 h to construct the HG injury model [32,33]. MPC5 in the NG+Rhein group was treated with 5.5 mM glucose, 24.5 mM mannitol, and 25 μg/mL rhein (extracted from the root of *Rheum palmatum* L of Polygonaceae) (98%, CAS#478-43-3, R7269, Sigma, USA) for 48 h [29]. MPC5 in the HG+Rhein group was treated with 30 mM HG and 25 μg/mL rhein for 48 h.

In experiment 2, MPC5 was divided into 3 groups: HG, si-NC, and si-Rac1. Before HG induction, Rac1 silencing (si-Rac1) plasmid and its negative control (si-NC) were transfected into MPC5 of the si-NC group and si-Rac1 group using Lipofectamine 2000 (11668019, Invitrogen, Carlsbad, CA, USA). Then, MPC5 in HG, si-NC, and si-Rac1 groups were treated with 30 mM HG for 48 h, respectively.

In experiment 3, MPC5 was divided into 4 groups: HG, HG+oe-NC, Rhein+oe-NC, and Rhein+oe-Rac1. Before HG induction, Rac1 overexpression (oe-Rac1) plasmid and its negative control (oe-NC) were transfected into MPC5 of the HG+oe-NC group, Rhein+oe-NC group, and Rhein+oe-Rac1 group using Lipofectamine 2000. MPC5 in the HG+oe-NC group was treated with 30 mM HG for 48 h. MPC5 in Rhein+oe-NC and Rhein+oe-Rac1 groups were treated with 30 mM HG and 25 μg/mL rhein for 48 h.

2.3 Construction of DN Model and Intervention

C57BL/6J male mice (6–8 weeks, 18–20 g) were bought from Hunan SJA Laboratory Animal Co., Ltd (Changsha, China). Mice were first accepted one week of adaptive feeding and then divided into 5 groups: Sham, DN, Rhein, Rhein+LV-NC, and Rhein+LV-Rac1, with 6 mice in each group. Mice in the DN group were intraperitoneally injected with STZ (50 mg/kg) (AWH0492, Abiowell, Changsha, China) and deprived of food for 4–6 h every day for 5 consecutive days. On day 3 after injection, the glucose level of tail blood was detected, and the DN model was constructed when it was greater than 16.7 mmol/L [34]. Mice in the Sham group were given the same dose of citrate buffer. Mice in the Rhein, Rhein+LV-NC, and Rhein+LV-Rac1 groups were gavaged with rhein at a dose of 150 mg/(kg·d) while the other groups were given the same dose of normal saline [20]. Besides, 2 weeks before STZ injection, mice in Rhein+LV-NC and Rhein+LV-Rac1 groups were injected with Rac1 Lentivirus (LV-Rac1) and its negative control (LV-NC) (titer 2×10^9 TU/mL) through the tail vein, respectively. The body weight and blood glucose levels of mice in different groups were measured before STZ intervention, on days 3, 7, 14, 21, and 28, respectively. Four weeks after the construction of the DN model, the mice

were sacrificed, and their blood, urine, and kidneys were collected for detection (fasting for 12 hours before sampling). The kidneys were fixed with 4% paraformaldehyde, embedded in paraffin, and sectioned for staining experiments. All procedures were approved by the Animal Experimental Ethical Committee of the First Hospital of Human University of Chinese Medicine (No. ZYFY20220223).

2.4 Cell Counting Kit-8 (CCK-8) Assay

CCK-8 kit was utilized to detect the viability of MPC5 in different groups. MPC5 in the logarithmic growth phase was digested by trypsin (AWC0232, Abiowell, Changsha, China) and counted. The cells were seeded in 96-well plates at a density of 5×10^3 cells/well, 100 μL per well. After cell adhesion, the cells were treated respectively. Then, 100 μL of medium containing 10% CCK-8 (NU679, DOJINDO, Kyushu, Japan) was added to each well, and cultured for another 4 h in a humidified incubator containing 5% CO_2 at 37 °C. Optical density (OD) at 450 nm was analyzed with a multifunctional microplate reader.

2.5 Flow Cytometry

Flow cytometry was applied to detect the levels of lipid ROS in different groups of MPC5. MPC5 was digested with trypsin to prepare the cell suspension. The cells were centrifuged at 2000 rpm for 5 min, then the supernatant was discarded followed by washing with PBS twice. C11-BODIPY (50 μM) (MX5211-1MG, MKBIO, Shanghai, China) was added and incubated at 37 °C for 1 h. The cells were washed twice with PBS and the supernatant was discarded. The precipitates were suspended in 300 μL PBS and detected by flow cytometry.

2.6 Immunofluorescence (IF) Staining

IF staining was used to detect the expression of GPX4, α-smooth muscle actin (α-SMA), and Nephrin in podocytes and Podocin in mouse kidneys. For renal tissue detection, the slices were first placed in xylene for 20 min for dewaxing. Dehydration was carried out with gradient ethanol (75–100%), 5 min for each level. The slices were then immersed in EDTA buffer (pH 9.0) and boiled for antigen repair. They were placed in sodium borohydride solution for 30 min and rinsed with tap water for 5 min. The slices were immersed in 75% ethanol solution for 1 min and then incubated in Sudan black dye solution for 15 min. After rinsing with tap water for 5 min, the slices were blocked with 5% BSA for 1 h. For podocyte detection, slides of cells were fixed with 4% paraformaldehyde for 30 min. After transparency with 0.3% triton at 37 °C for 30 min, the slides of cells were washed with PBS for 3 min. Then, they were blocked with 5% BSA at 37 °C for 1 h and rinsed with PBS for 3 min. The tissue slices were incubated with the primary antibody of Podocin (20384-1-AP, PTG, Chicago, IL, USA) overnight at 4 °C. The slides of cells were incubated with primary antibodies of GPX4 (67763-1-IG, Proteintech, Chicago, IL, USA), α-SMA (55135-1-AP, Proteintech, Chicago, IL, USA), and Nephrin (Ab216341, Abcam, Cambridge, UK) overnight at 4 °C. Then 100 μL CoraLite488-conjugated AffiniPure Goat Anti-Rabbit IgG (SA00013-2, Proteintech, Chicago, IL, USA) or CoraLite594-conjugated Affinipure Goat Anti-Mouse IgG (SA00013-4, Proteintech, Chicago, IL, USA) was added separately and incubated for 1.5 h at 37 °C. The nucleus was stained with DAPI (AWI0331a, Abiowell, Changsha, China) at 37 °C for 20 min. The tissue slices and slides of cells were sealed with glycerin and observed under a fluorescence microscope.

2.7 Hematoxylin-Eosin (HE) Staining

HE staining was used to detect renal morphological lesions in different groups of mice. First, the slices were dewaxed by placing them in xylene for 20 min. Then dehydration was carried out with gradient ethanol (75–100%), 5 min for each level. The slices were stained with hematoxylin (AWI0001a, Abiowell, Changsha, China) for 1 min, rinsed with distilled water, and then returned to blue in PBS. Next, the slices were stained with eosin (AWI0029a, Abiowell, Changsha, China) for 1 min and rinsed with distilled water. Dehydration was carried out with gradient alcohol (95–100%), 5 min for each level. The slices were cleared in xylene for 10 min and then sealed with neutral gum (AWI0238a, Abiowell, Changsha, China) for observation by microscope.

2.8 Immunohistochemistry (IHC) Staining

IHC staining was applied to detect the expression of α-SMA and Nephrin in the kidneys of different groups of mice. First, the slices were dewaxed by placing them in xylene for 20 min. Then dehydration was carried out with gradient ethanol (75–100%), 5 min for each level. The slices were immersed in citrate buffer (0.01 M, pH 6.0) (AWI0206a, Abiowell, Changsha, China), and boiled for antigen repair. Subsequently, 1% periodic acid was added to inactivate the endogenous enzyme. The slices were incubated with antibodies of α-SMA (55135-1-AP, Proteintech, Chicago, IL, USA) and Nephrin (Ab216341, Abcam, Cambridge, UK) overnight at 4 °C separately. Then, the slices were incubated with 100 μL HRP-anti-Rabbit-IgG for 30 min at 37 °C. Next, 100 μL DAB was added to slices and incubated for 5 min for color development. The slices were counterstained with hematoxylin for 5 min, rinsed with distilled water, and returned to blue in PBS. Dehydration was carried out with gradient alcohol (60–100%), 5 min for each level. The slices were cleared in xylene for 10 min and then sealed with neutral gum for observation by microscope.

2.9 Masson Staining

Renal tubulointerstitial fibrosis in different groups of mice was detected by Masson staining. First, the renal slices were dewaxed to water. Hematoxylin stain solution was added to cover the slices and then stained for 1 min.

The slices were washed with tap water and distilled water in turn. Then, the slices were soaked in PBS (pH 7.2–7.6) or ammonia for 10 min to make the nucleus return blue. Acid fuchsin stain solution was added and stained for 5 min. After that, the slices were reacted with a phosphomolybdic acid differentiation solution for about 30 s. The tissue was covered by a drop of aniline blue counterstain, stained for 3 min, and rinsed with absolute ethanol. The slices were blow-dried, cleared in xylene, and then sealed with neutral gum for observation by microscope.

2.10 Biochemical Detection

According to the instructions of the superoxide dismutase (SOD) assay kit (A001-3, NJJCBIO, Nanjing, China), malondialdehyde (MDA) assay kit (A003-1, NJJCBIO, Nanjing, China), reduced glutathione (GSH) assay kit (A006-2-1, NJJCBIO, Nanjing, China), iron assay kit (ab83366, Abcam, Cambridge, UK), creatinine assay kit (C011-2-1, NJJCBIO, Nanjing, China), blood urea nitrogen (BUN) assay kit (C013-2-1, NJJCBIO, Nanjing, China), urinary albumin quantitative assay kit (C035-2-1, NJJCBIO, Nanjing, China), glucose assay kit (F006, NJJCBIO, Nanjing, China), respectively, the contents of SOD, MDA, GSH, Fe^{2+}, creatinine, BUN, urinary albumin, and blood glucose in experimental samples were measured.

2.11 Quantitative Real-Time Polymerase Chain Reaction (RT-qPCR)

RT-qPCR was employed to measure the expression of Rac1, NOX1, β-catenin, E-cadherin, Vimentin, Snail, and Desmin in different groups of MPC5. Firstly, total RNA was extracted by using the Trizol total RNA extraction kit (15596026, Thermo, Waltham, MA, USA). mRNA was reverse transcribed into cDNA according to the guidance of the mRNA reverse transcription kit (CW2569, CWBIO, Beijing, China), followed by RT-qPCR. The primers used were as follows: β-actin: F: ACCCTGAAGTACCCCATCGAG, R: AGCACAGCCTGGATAGCAAC; Rac1: F: TGACCCTCTTTACCTCGCCCAC, R: AACATCGTCAGCACTAGCACAG; NOX1: F: TAAAGGCTCACAGACCCTGC, R: GAGCCCTTCTAGGCAACAGG; β-catenin: F: ATTCTTGGCTATTACGACAGACT, R: AGCAGACAGATAGCACCTT; E-cadherin: F: AGCCATTGCCAAGTACATCCTC, R: CGCCTTCTGCAACGAATCCC; Vimentin: F: GTCCACACGCACCTACAGTCT, R: AAGTCCACCGAGTCTTGAAGC; Snail: F: TGCTTTTGCTGACCGCTCCAAC, R: GCACTGGTATCTCTTCACATCCGAGT; Desmin: F: CCATTGCCCTGGGATGAACT, R: GACTGTCCCCATCCCTACCT. The expression levels of target genes were calculated by the $2^{-\Delta\Delta Ct}$ method with β-actin as the internal reference.

2.12 Western Blotting

Western blotting was utilized to detect the expression of Recombinant Solute Carrier Family 7, Member 11 (SLC7A11), Transferrin Receptor 1 (TFR1), acyl-CoA synthetase long-chain family member 4 (ACSL4), E-cadherin, Vimentin, Snail, Desmin, Rac1, NOX1, β-catenin, and GPX4. Different groups of samples were treated with RIPA lysate (AWB0136, Abiowell, Changsha, China) to extract total proteins. The protein was separated by SDS-PAGE and transferred to the nitrocellulose (NC) membrane. The NC membrane was blocked with 5% skimmed milk (AWB0004, Abiowell, Changsha, China) for 1.5 h and then incubated with primary antibodies at 4 °C overnight separately. Primary antibodies were as followed: SLC7A11 (1:1,000, 26864-1-AP, Proteintech, Chicago, IL, USA), TFR1 (1:5,000, ab269513, Abcam, Cambridge, UK), ACSL4 (1:10,000, ab155282, Abcam, Cambridge, UK), E-cadherin (1:5,000, 20874-1-AP, Proteintech, Chicago, IL, USA), Vimentin (1:5,000, 10366-1-AP, Proteintech, Chicago, IL, USA), Snail (1:500, 13099-1-AP, Proteintech, Chicago, IL, USA), Desmin (1:10,000, 16520-1-AP, Proteintech, Chicago, IL, USA), Rac1 (1:500, 24072-1-AP, Proteintech, Chicago, IL, USA), NOX1 (1:1,000, 17772-1-AP, Proteintech, Chicago, IL, USA), β-catenin (1:10,000, 51067-2-AP, Proteintech, Chicago, IL, USA), GPX4 (1:1,000, 67763-1-Ig, Proteintech, Chicago, IL, USA), and β-actin (1:5,000, 66009-1-Ig, Proteintech, Chicago, IL, USA). The NC membrane was incubated with HRP-goat anti-mouse IgG (1:5,000, SA00001-1, Proteintech, Chicago, IL, USA) or HRP-goat anti-rabbit IgG (1:6,000, SA00001-2, Proteintech, Chicago, IL, USA) for 1.5 h. Finally, the NC membrane was incubated with ECL reagent (AWB0005, Abiowell, Changsha, China) and followed by imaging. The expression levels of each protein were analyzed by Quantity One 4.6.6 (Bio-Rad Inc., Hercules, CA, USA) with β-actin as the reference protein.

2.13 Data Analysis

GraphPad Prism 8.0 (GraphPad Software Inc., San Diego, CA, USA) was used for data analysis. Experimental data were expressed as mean $\pm$ standard deviation (SD). One-way analysis of variance (one-way ANOVA) and two-way analysis of variance (two-way ANOVA) were used for comparison between groups, and $p < 0.05$ was considered statistically significant.

3. Results

3.1 Rhein Inhibited HG-Induced Ferroptosis in Podocytes

To screen the suitable concentration of rhein, podocytes were treated with a range of concentrations of rhein (0, 5, 15, 25, 50, and 100 μg/mL) for 24 h and 48 h. The half maximal inhibitory concentration (IC_{50}) of rhein at 24 and 48 h was 115.92 μg/mL and 89.14 μg/mL,

respectively (Fig. 1A). When the concentration of rhein exceeded 25 μg/mL, its inhibitory effect on podocyte proliferation was very significant, so it was selected to carry out follow-up experiments. To investigate the effect of rhein on HG-induced ferroptosis in podocytes, we first constructed the HG injury model and co-cultured it with rhein for 48 h. CCK-8 detection results in Fig. 1B displayed that podocytes viability in the HG group was obviously reduced, indicating the HG injury model was successfully constructed. However, the viability of HG-treated podocytes was recovered by co-culture with rhein. Moreover, flow cytometry further revealed that rhein reduced HG-induced lipid ROS accumulation (Fig. 1C). Next, biochemical detection results displayed that rhein reduced the content of MDA and Fe^{2+} in HG-treated podocytes, but promoted the synthesis and accumulation of SOD and GSH (Fig. 1D). It was found by IF staining that rhein co-culture reversed the inhibitory effect of HG on GPX4 synthesis in podocytes (Fig. 1E). The expression of SLC7A11 in HG-treated podocytes was increased after co-culture with rhein, while TFR1 and ACSL4 were the opposite (Fig. 1F). These results indicated that rhein could inhibit HG-induced ferroptosis in podocytes.

3.2 Rhein Inhibited HG-Induced EMT in Podocytes

We then investigated the effect of rhein on HG-induced EMT in podocytes. Podocytes were subjected to HG and co-cultured with rhein for 48 h, and the expression of the marker proteins of EMT was analyzed. As shown in Fig. 2A, α-SMA content decreased while Nephrin content increased in HG-treated podocytes after co-culture with rhein. It was further found that rhein significantly inhibited the expression of Vimentin, Snail, and Desmin at the mRNA and protein levels in HG-treated podocytes. Moreover, rhein intervention promoted the high expression of E-cadherin in HG-treated podocytes (Fig. 2B). These results indicated that rhein could inhibit HG-induced EMT in podocytes.

3.3 Rhein Inhibited the Rac1 Pathway

To further investigate the specific mechanism of rhein in alleviating HG-induced podocyte injury, we analyzed the expression of Rac1 and its downstream targets NOX1 and β-catenin respectively. As displayed in Fig. 3A, the mRNA expression levels of Rac1, NOX1, and β-catenin in HG-treated podocytes were significantly decreased after rhein intervention. Consistently, the protein expression levels of Rac1, NOX1, and β-catenin were also downregulated in response to rhein (Fig. 3B). Together, these results indicated that rhein could inhibit the Rac1 pathway.

3.4 Rac1 Pathway Activation Mediated HG-Induced Ferroptosis and EMT in Podocytes

To explore the role of the Rac1 pathway in HG-induced ferroptosis and EMT, podocytes were transfected with si-Rac1 first and then treated with HG. Western blotting results displayed that si-Rac1 significantly decreased the expression of Rac1 and its downstream targets NOX1 and β-catenin (Fig. 4A). In addition, biochemical detection results displayed that si-Rac1 reduced MDA and Fe^{2+} contents in HG-treated podocytes, but significantly promoted the synthesis and accumulation of SOD and GSH (Fig. 4B). By Western blotting analysis of ferroptosis-related proteins, we further found that the expression of SLC7A11 and GPX4 in HG-treated podocytes was significantly increased after si-Rac1 transfection, while TFR1 and ACSL4 were opposite (Fig. 4C). In addition, the IF staining of the marker proteins of EMT revealed that the EMT in HG-treated podocytes was inhibited under the action of si-Rac1, which was manifested as the decrease of α-SMA and the increase of Nephrin (Fig. 4D). These results indicated that Rac1 pathway activation could mediate HG-induced ferroptosis and EMT in podocytes.

3.5 Rhein Inhibited HG-Induced Ferroptosis and EMT in Podocytes by Regulating the Rac1 Pathway

To further determine the role of rhein in inhibiting HG-induced ferroptosis and EMT in podocytes by regulating the Rac1 pathway *in vitro*, podocytes were transfected with oe-Rac1 before HG induction and rhein intervention. As shown in the biochemical detection results in Fig. 5A, the contents of MDA and Fe^{2+} in podocytes co-cultured with rhein decreased remarkably while the contents of SOD and GSH increased. However, oe-Rac1 transfection reversed the inhibitory effect of rhein on HG-induced ferroptosis. In addition, Western blotting results displayed that rhein inhibited the HG-induced overexpression of TFR1 and ACSL4. However, oe-Rac1 transfection displayed the opposite result, with upregulated expression of TFR1 and ACSL4 and downregulated expression of SLC7A11 and GPX4 (Fig. 5B). IF staining detection further revealed that rhein inhibited HG-induced EMT in podocytes, but oe-Rac1 transfection reversed this situation, resulting in increased α-SMA content and decreased Nephrin content (Fig. 5C). These results indicated that rhein could inhibit HG-induced ferroptosis and EMT in podocytes by regulating the Rac1 pathway.

3.6 Rhein Inhibited Ferroptosis and EMT in DN Mice by Regulating the Rac1 Pathway

To further explore the role of rhein in inhibiting DN-induced ferroptosis and EMT by regulating the Rac1 pathway *in vivo*, LV-Rac1 was injected through the tail vein of mice 2 weeks before the construction of the DN model, and then rhein was administered by gavage. Compared with the Sham group, the body weight of mice in the DN group was sharply decreased, accompanied by persistent hyperglycemia, indicating that the DN model was successfully constructed. Mice in the Rhein group had higher body weight and lower blood glucose than those in the

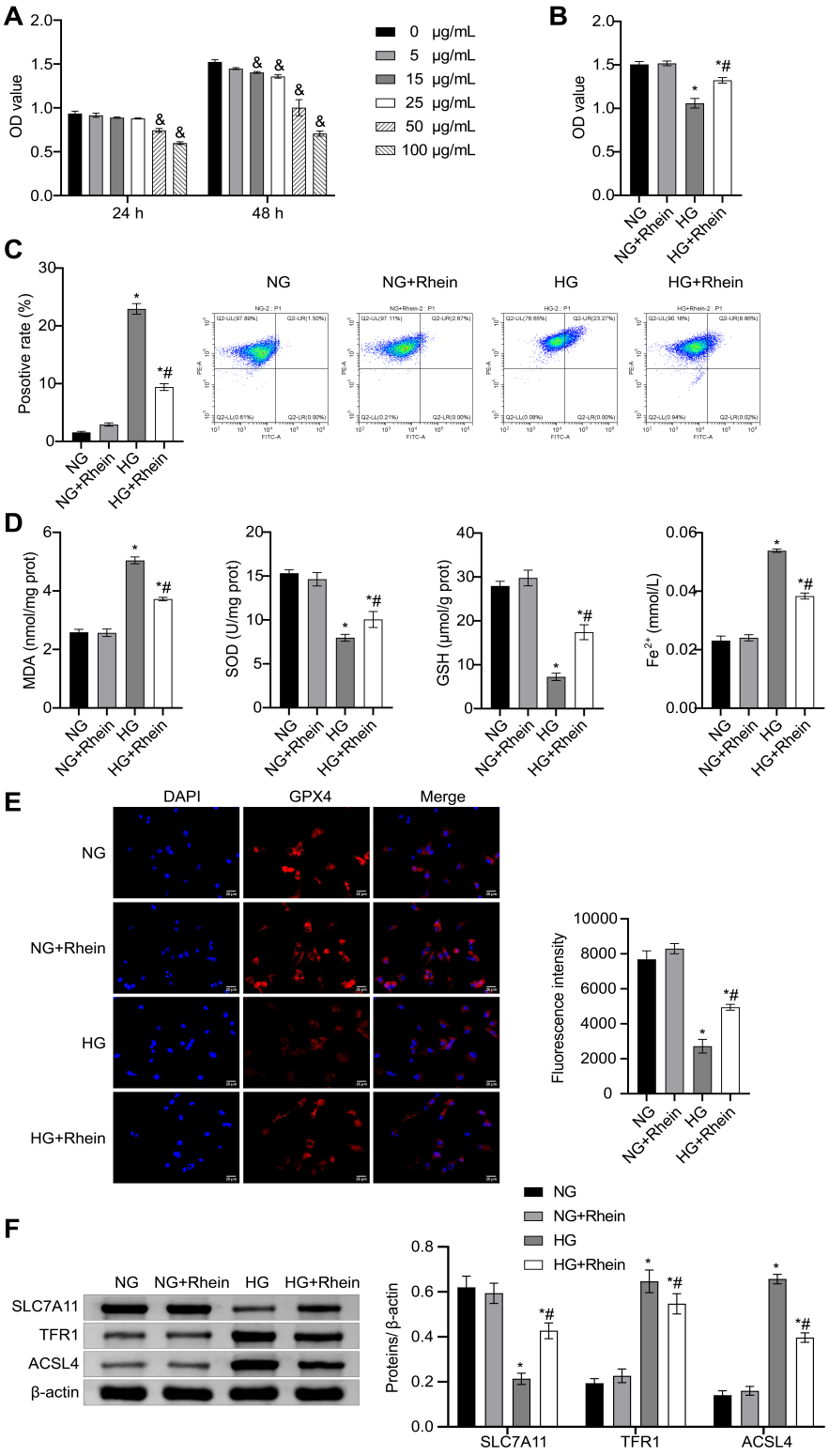

Fig. 1. Rhein inhibited HG-induced ferroptosis in podocytes. (A,B) CCK-8 assay of podocytes viability. (C) Flow cytometry detection of lipid ROS levels. (D) Biochemical detection of MDA, SOD, GSH, and Fe^{2+} contents. (E) IF staining detection of GPX4 content. (F) Western blotting analysis of SLC7A11, TFR1, ACSL4 expressions. & $p < 0.05$ vs. 0 μg/mL, * $p < 0.05$ vs. NG, # $p < 0.05$ vs. HG, one-way ANOVA, two-way ANOVA. Notes: IC_{50}, half maximal inhibitory concentration; NG, normal glucose; HG, high glucose; CCK-8, Cell Counting Kit-8; ROS, reactive oxygen species; MDA, malondialdehyde; SOD, superoxide dismutase; GSH, glutathione; IF, immunofluorescence; SLC7A11, Recombinant Solute Carrier Family 7, Member 11; TFR1, Transferrin Receptor 1; ACSL4, acyl-CoA synthetase long-chain family member 4.

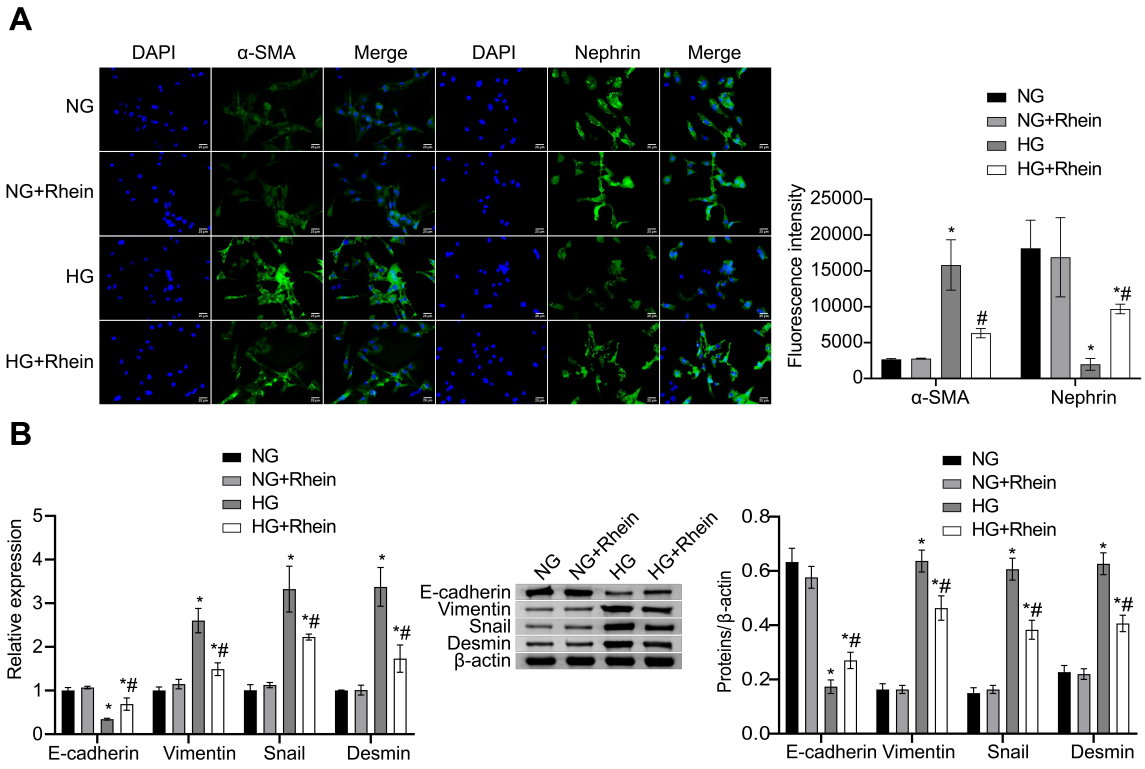

Fig. 2. Rhein inhibited HG-induced EMT in podocytes. (A) IF staining detection of α-SMA and Nephrin contents. (B) RT-qPCR and Western blotting analysis of E-cadherin, Vimentin, Snail, and Desmin expressions. * $p < 0.05$ vs. NG, # $p < 0.05$ vs. HG, one-way ANOVA. Notes: NG, normal glucose; HG, high glucose; EMT, epithelial-mesenchymal transition; IF, immunofluorescence; α-SMA, α-smooth muscle actin; RT-qPCR, quantitative real-time polymerase chain reaction.

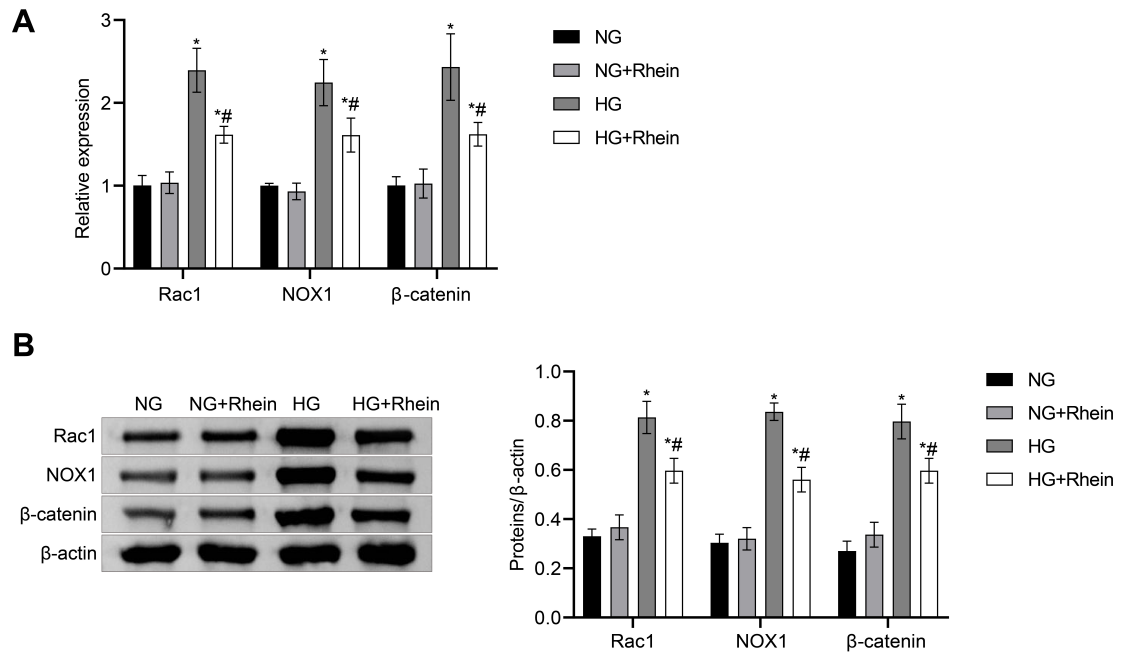

Fig. 3. Rhein inhibited the Rac1 pathway. RT-qPCR (A) and Western blotting (B) analysis of Rac1, NOX1, and β-catenin expressions. * $p < 0.05$ vs. NG, # $p < 0.05$ vs. HG, one-way ANOVA. Notes: NG, normal glucose; HG, high glucose; Rac1, Ras-related C3 botulinum toxin substrate 1; NOX1, NADPH Oxidase 1; RT-qPCR, quantitative real-time polymerase chain reaction.

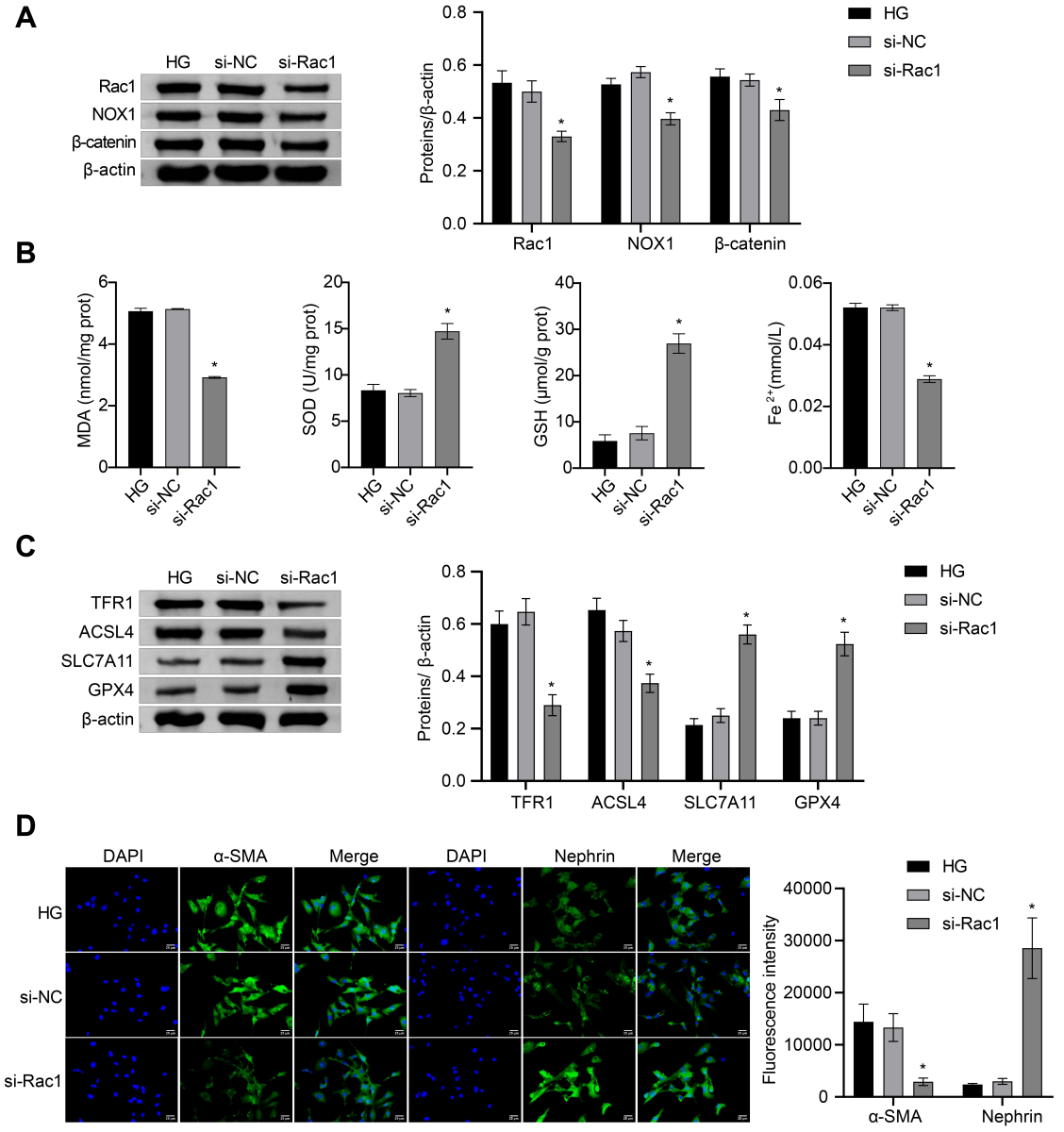

Fig. 4. Rac1 pathway activation mediated HG-induced ferroptosis and EMT in podocytes. (A) Western blotting analysis of Rac1, NOX1, and β-catenin expressions. (B) Biochemistry detection of MDA, SOD, GSH, and Fe^{2+} contents. (C) Western blotting analysis of TFR1, ACSL4, SLC7A11, and GPX4 expressions. (D) IF staining detection of α-SMA and Nephrin contents. * $p < 0.05$ vs. HG, one-way ANOVA. Notes: HG, high glucose; si, silencing; NC, negative control; Rac1, Ras-related C3 botulinum toxin substrate 1; EMT, epithelial-mesenchymal transition; NOX1, NADPH Oxidase 1; MDA, malondialdehyde; SOD, superoxide dismutase; GSH, glutathione; TFR1, Transferrin Receptor 1; ACSL4, acyl-CoA synthetase long-chain family member 4; SLC7A11, Recombinant Solute Carrier Family 7, Member 11; GPX4, glutathione peroxidase 4; IF, immunofluorescence; α-SMA, α-smooth muscle actin.

DN group, but LV-Rac1 injection changed these conditions (Fig. 6A). The renal index and urinary albumin levels of mice in the DN group were significantly higher than those in the Sham group, which verified the successful induction of DN. In addition, LV-Rac1 injection significantly inhibited the relieving effect of rhein on DN (Fig. 6B). Biochemical detection results displayed that rhein intervention significantly reduced DN-induced high BUN and serum creatinine, whereas LV-Rac1 injection presented the opposite result (Fig. 6C). Furthermore, HE staining displayed thickened GBM and hypertrophic glomeruli in DN mice. Masson staining displayed marked renal tubulointerstitial fibrosis in DN mice. These conditions were alleviated by rhein intervention. However, the injection of LV-Rac1 reversed the therapeutic effect of rhein on DN (Fig. 6D). Using IF staining, Podocin content was further found to be significantly increased after rhein intervention but significantly decreased after LV-Rac1 injection (Fig. 6E). West-

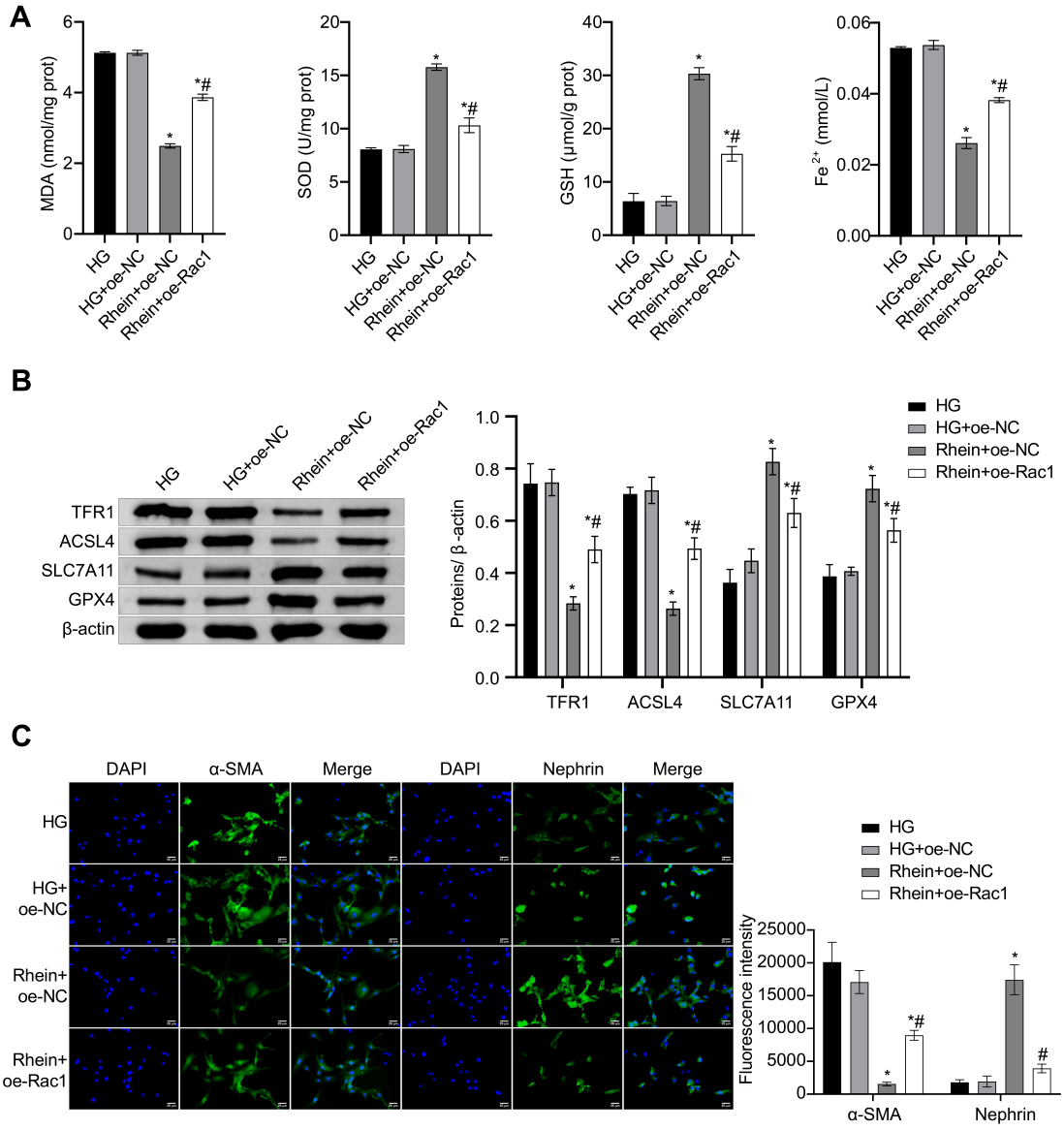

Fig. 5. Rhein inhibited HG-induced ferroptosis and EMT in podocytes by regulating the Rac1 pathway. (A) Biochemical detection of MDA, SOD, GSH, and Fe^{2+} contents. (B) Western blotting analysis of TFR1, ACSL4, SLC7A11, and GPX4 expressions. (C) IF staining detection of α-SMA and Nephrin contents. * $p < 0.05$ vs. HG, # $p < 0.05$ vs. Rhein+oe-NC, one-way ANOVA. Notes: HG, high glucose; oe, overexpression; NC, negative control; EMT, epithelial-mesenchymal transition; Rac1, Ras-related C3 botulinum toxin substrate 1; MDA, malondialdehyde; SOD, superoxide dismutase; GSH, glutathione; TFR1, Transferrin Receptor 1; ACSL4, acyl-CoA synthetase long-chain family member 4; SLC7A11, Recombinant Solute Carrier Family 7, Member 11; GPX4, glutathione peroxidase 4; IF, immunofluorescence; α-SMA, α-smooth muscle actin.

ern blotting results revealed that GPX4 and SLC7A11 were highly expressed and RAC1, NOX1, β-catenin, TFR1, and ACSL4 were lowly expressed in the Rhein group. However, the expression of these proteins was opposed in the Rhein+LV-Rac1 group (Fig. 6F,H). In addition, Rhein intervention inhibited the accumulation of MDA and Fe^{2+} but significantly promoted the synthesis of SOD and GSH. However, LV-Rac1 injection reversed this trend (Fig. 6G). IHC staining further found that the content of α-SMA was low and the content of Nephrin was high in the Rhein group, while the situation was opposite in the Rhein+LV-Rac1 group (Fig. 6I). These results indicated that rhein inhibited ferroptosis and EMT in DN mice by regulating the Rac1 pathway.

4. Discussion

In the study of DN, both ferroptosis and EMT have been involved in the progression of DN. With in-depth exploration, it has been found that rhein, as the main extract of rhubarb, has a potential therapeutic effect on DN [35].

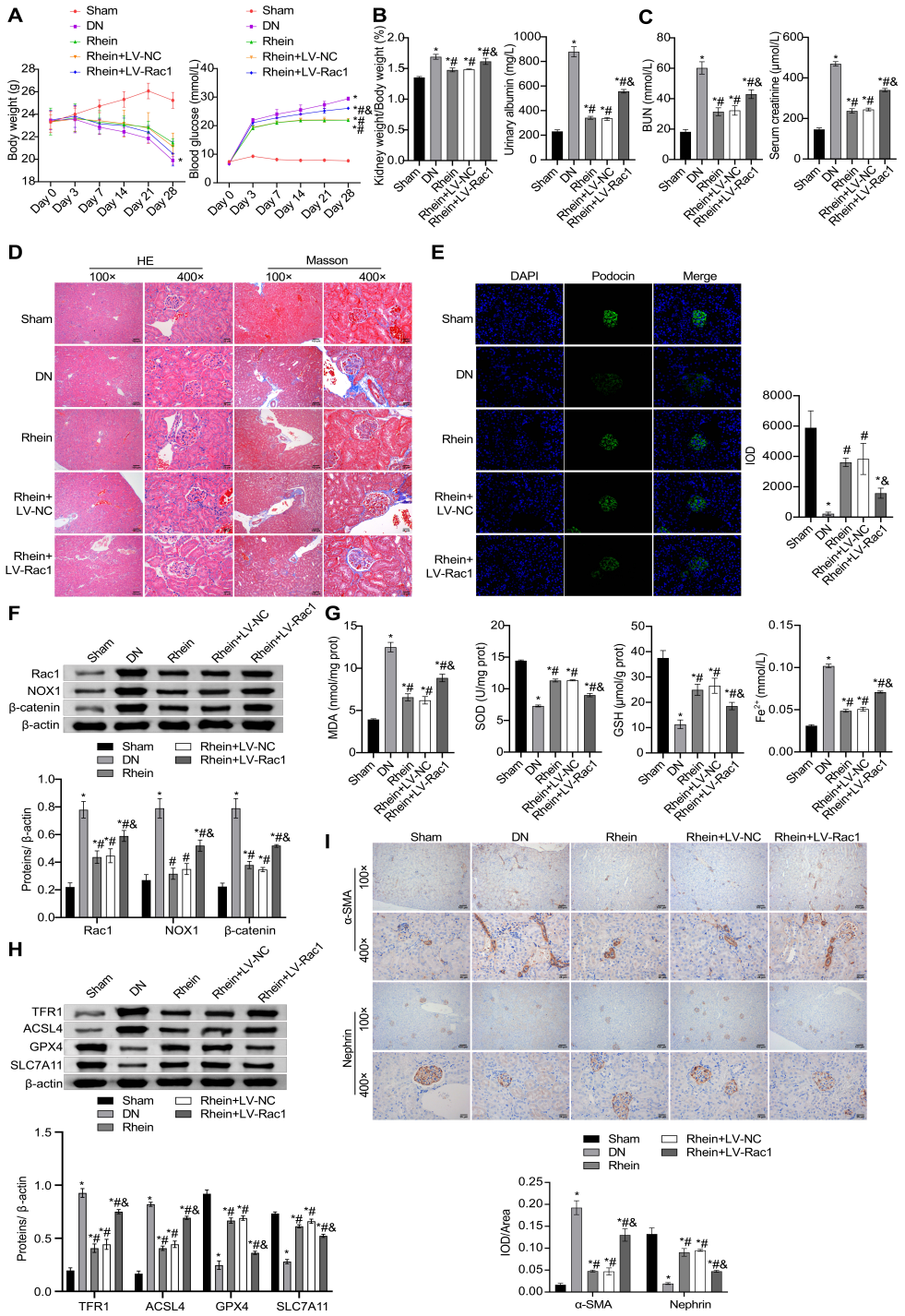

Fig. 6. Rhein inhibited ferroptosis and EMT in DN mice by regulating the Rac1 pathway. (A) Body weight and blood glucose. (B) Renal index and urinary albumin level. (C) Biochemical detection of BUN and serum creatinine contents. (D) HE staining and Masson staining. (E) IF staining detection of Podocin content. (F) Western blotting analysis of Rac1, NOX1, and β-catenin expressions. (G) Biochemical detection of MDA, SOD, GSH, and Fe^{2+} contents. (H) Western blotting analysis of TFR1, ACSL4, SLC7A11, and GPX4 expressions. (I) IHC staining detection of α-SMA and Nephrin contents. * $p < 0.05$ vs. Sham; # $p < 0.05$ vs. DN, & $p < 0.05$ vs. Rhein+LV-NC, one-way ANOVA, two-way ANOVA. Notes: EMT, epithelial-mesenchymal transition; DN, diabetic nephropathy; LV, Lentivirus; NC, negative control; Rac1, Ras-related C3 botulinum toxin substrate 1; BUN, blood urea nitrogen; HE, Hematoxylin-eosin; IF, immunofluorescence; NOX1, NADPH Oxidase 1; MDA, malondialdehyde; SOD, superoxide dismutase; GSH, glutathione; TFR1, Transferrin Receptor 1; ACSL4, acyl-CoA synthetase long-chain family member 4; SLC7A11, Recombinant Solute Carrier Family 7, Member 11; GPX4, glutathione peroxidase 4; IHC, immunohistochemistry; α-SMA, α-smooth muscle actin.

However, the specific mechanism of rhein in improving DN remains to be explored. Here we studied the effect of rhein on DN by constructing a podocyte HG model and mouse DN model and further analyzed the specific mechanism of Rac1 and its downstream NOX1/β-catenin pathway in the inhibition of DN development by rhein.

Ferroptosis is involved in the pathological process of serious diseases, including tumors, cardiovascular and cerebrovascular diseases, neurodegenerative diseases, and renal diseases [36]. ROS accumulation and iron overload in ferroptosis are important determinants in DN development [6]. Previous studies proved that iron accumulation increased DN-induced renal injury by increasing oxidative stress or decreasing antioxidant capacity [8]. In DN, massive ROS is produced due to the disorder of glucose metabolism, which induces renal structural and functional damage. Meanwhile, abnormal lipid metabolism leads to the accumulation of MDA [5]. Due to the sensitivity of podocytes to ROS, excessive ROS can cause irreversible changes in podocyte structure and function [37]. In this study, HG-induced podocytes produced massive ROS, and MDA, and inhibited the synthesis and accumulation of SOD and GSH. However, rhein intervention noticeably repaired HG-induced damage in podocytes. In the study of rhein, it was found that rhein could protect cells from H_2O_2-induced damage, reduce the content of MDA, and increase the activities of SOD and GSH-PX [38]. Here we found HG-induced ferroptosis in podocytes, as shown by the increase of Fe^{2+}, TFR1, and ACSL4 and the decrease of GPX4 and SLC7A11, which were consistent with previous studies [26]. However, HG-induced podocyte ferroptosis was inhibited in the presence of rhein. The catalytic activity of GPX4 contributes to reducing the level of lipid peroxidation to inhibit the occurrence of ferroptosis [39]. SLC7A11 is involved in the exchange of extracellular cystine and glutamate and plays an inhibitory role in ferroptosis. Related studies have shown that activation of the SLC7A11/GPX4 axis can inhibit ferroptosis [40]. TFR1 is considered a marker protein for the occurrence of ferroptosis, which can be prevented by a TFR1 inhibitor or knockdown of TFR1 [41]. ACSL4 is a known promoter of ferroptosis, and knockdown of it has a protective effect against ferroptosis-mediated acute renal injury [42].

Studies have shown that EMT is one of the important mechanisms of renal tubulointerstitial fibrosis in the progression of renal lesions [43,44]. Podocytes may undergo phenotypic transformation through EMT under certain injuries. Therefore, the occurrence of EMT in podocytes may be one of the important mechanisms of podocyte loss in DN [45]. When EMT occurs, epithelial-like phenotypic markers such as E-cadherin are lost, and mesenchymal phenotypic markers such as Vimentin and α-SMA are expressed [46]. Snail is an important promoter of the EMT process and can directly inhibit E-cadherin expression at the transcriptional level [47]. In the present study, the expressions of α-SMA, Vimentin, Snail, and Desmin were up-regulated and those of E-cadherin and Nephrin were down-regulated in HG-treated podocytes. Rhein could antagonize EMT and reverse the above trends, which were consistent with the results of related studies [48]. These results suggest rhein could be effective in the treatment of DN by inhibiting EMT in podocytes.

Aberrant activation of Rac1 plays an important role in renal diseases [49]. During DN pathogenesis, Rac1 overactivation induces changes in podocyte structure and function [50]. Here, HG activated the Rac1 pathway in podocytes and promoted the high expression of downstream NOX1 and β-catenin, but it was inhibited in the presence of rhein intervention. Besides, si-Rac1 transfection verified that the activation of the Rac1 pathway mediated ferroptosis and EMT in HG-induced podocytes. In addition, *in vitro* results displayed that DN mice had decreased body weight, increased blood glucose, and high renal index. However, the symptoms were relieved under rhein gavage treatment. A high glucose environment is an important cause of diabetic complications. Therefore, controlling blood glucose can reduce the incidence of DN [51]. Moreover, the biochemical detection results displayed that the levels of urinary albumin, BUN, and serum creatinine in DN mice were high, which was consistent with the performance of DN in the literature [52,53]. However, these symptoms were relieved by rhein treatment. In related studies, it was found that rhein could inhibit the wnt/β-catenin signaling pathway and increase Nephrin expression in podocytes of db/db mice, to reduce the excretion of urinary albumin and repair HG-induced podocyte injury [29]. HE staining and Masson staining further revealed that GBM thickening, glomerular hypertrophy, and renal tubulointerstitial fibrosis were observed in DN mice, which were relieved after rhein intervention. In DN, GBM thickening is one of the main features [54]. The appearance of renal tubulointerstitial fibrosis results in renal dysfunction [12]. In previous studies, rhein improved the autophagy of mouse renal tubular cells and delayed the progression of renal tubulointerstitial fibrosis by regulating the AMPK/mTOR signaling pathway [55]. Podocin is an important protein in the hiatal membrane of podocytes, which can maintain the structure and function of podocytes. Here, Podocin expression was reduced in kidney tissue of DN mice but was rescued by rhein intervention. In addition, overexpression of Rac1 reversed the protective effect of rhein against renal injury. These results suggested that rhein inhibited ferroptosis and EMT in DN mice through the Rac1 pathway.

5. Conclusions

In conclusion, our findings suggested that rhein could effectively alleviate DN. In terms of mechanism, rhein inhibited the development of DN by regulating the Rac1/NOX1/β-catenin axis *in vitro* and *in vivo* to inhibit ferroptosis and EMT. This study will provide a scientific

basis for rhein in the treatment of DN and further study of its mechanism.

Availability of Data and Materials

All raw data can be obtained from the corresponding author.

Author Contributions

Conceptualization—DX and WH. Methodology—DX, WH, and XH. Data Curation and Formal Analysis—YC. Visualization. DX and WH. Writing the Original Draft—WH. All authors contributed to editorial changes in the manuscript. All authors read and approved the final manuscript. All authors have participated sufficiently in the work and agreed to be accountable for all aspects of the work.

Ethics Approval and Consent to Participate

All procedures were approved by the Animal Experimental Ethical Committee of the First Hospital of Human University of Chinese Medicine (No. ZYFY20220223).

Acknowledgment

Not applicable.

Funding

This study was supported by Natural Science Foundation of Hunan Province (No. 2020JJ5439); Hunan Clinical Medical Technology Innovation and Guidance Project (No. 2021SK51418); Key Nursing Project of Hunan University of Traditional Chinese Medicine (No. 2019XJJJ072); Chinese Medicine Inheritance And Innovation Project of Backbone Talents of Western Medicine learn Traditional Chinese Medicine (No. 08-01-03).

Conflict of Interest

The authors declare no conflict of interest.

References

[1] Drummond K, Mauer M. The early natural history of nephropathy in type 1 diabetes: II. Early renal structural changes in type 1 diabetes. Diabetes. 2002; 51: 1580–1587.

[2] Gilbert RE, Cooper ME. The tubulointerstitium in progressive diabetic kidney disease: more than an aftermath of glomerular injury? Kidney International. 1999; 56: 1627–1637.

[3] Collins AJ, Kasiske B, Herzog C, Chavers B, Foley R, Gilbertson D, *et al*. Excerpts from the United States Renal Data System 2006 Annual Data Report. American Journal of Kidney Diseases. 2007; 49: A6–A7, S1–S296.

[4] Pavenstädt H, Kriz W, Kretzler M. Cell biology of the glomerular podocyte. Physiological Reviews. 2003; 83: 253–307.

[5] Feng X, Wang S, Sun Z, Dong H, Yu H, Huang M, *et al*. Ferroptosis Enhanced Diabetic Renal Tubular Injury *via* HIF-1α/HO-1 Pathway in db/db Mice. Frontiers in Endocrinology. 2021; 12: 626390.

[6] Li S, Zheng L, Zhang J, Liu X, Wu Z. Inhibition of ferroptosis by up-regulating Nrf2 delayed the progression of diabetic nephropathy. Free Radical Biology & Medicine. 2021; 162: 435–449.

[7] Hirschhorn T, Stockwell BR. The development of the concept of ferroptosis. Free Radical Biology & Medicine. 2019; 133: 130–143.

[8] Zou C, Liu X, Liu R, Wang M, Sui M, Mu S, *et al*. Effect of the oral iron chelator deferiprone in diabetic nephropathy rats. Journal of Diabetes. 2017; 9: 332–340.

[9] Yin J, Wang Y, Chang J, Li B, Zhang J, Liu Y, *et al*. Apelin inhibited epithelial-mesenchymal transition of podocytes in diabetic mice through downregulating immunoproteasome subunits β5i. Cell Death & Disease. 2018; 9: 1031.

[10] Liu Y. Epithelial to mesenchymal transition in renal fibrogenesis: pathologic significance, molecular mechanism, and therapeutic intervention. Journal of the American Society of Nephrology. 2004; 15: 1–12.

[11] Dai H, Liu Q, Liu B. Research Progress on Mechanism of Podocyte Depletion in Diabetic Nephropathy. Journal of Diabetes Research. 2017; 2017: 2615286.

[12] A/L B Vasanth Rao VR, Tan SH, Candasamy M, Bhattamisra SK. Diabetic nephropathy: An update on pathogenesis and drug development. Diabetes & Metabolic Syndrome. 2019; 13: 754–762.

[13] Pandiri I, Moni A. Ocimum herb species: A potential treatment strategy for diabetic kidney disease. Journal of Advanced Biotechnology and Experimental Therapeutics. 2018; 1: 88–91.

[14] Wang L, Li D, Bao C, You J, Wang Z, Shi Y, *et al*. Ultrasonic extraction and separation of anthraquinones from *Rheum palmatum* L. Ultrasonics Sonochemistry. 2008; 15: 738–746.

[15] Fan Y, Niu Z, Xu C, Yang L, Yang T. Protic Ionic Liquids as Efficient Solvents in Microwave-Assisted Extraction of Rhein and Emodin from *Rheum palmatum* L. Molecules. 2019; 24: 2770.

[16] Zhou Y, Xia W, Yue W, Peng C, Rahman K, Zhang H. Rhein: A Review of Pharmacological Activities. Evidence-based Complementary and Alternative Medicine. 2015; 2015: 578107.

[17] Zheng J, Zhu J, Li L, Liu Z. Rhein reverses the diabetic phenotype of mesangial cells over-expressing the glucose transporter (GLUT1) by inhibiting the hexosamine pathway. British Journal of Pharmacology. 2008; 153: 1456–1464.

[18] Jia ZH, Liu ZH, Zheng JM, Zeng CH, Li LS. Combined therapy of rhein and benazepril on the treatment of diabetic nephropathy in db/db mice. Experimental and Clinical Endocrinology & Diabetes. 2007; 115: 571–576.

[19] Cheng L, Chen Q, Pi R, Chen J. A research update on the therapeutic potential of rhein and its derivatives. European Journal of Pharmacology. 2021; 899: 173908.

[20] Gao Q, Qin W, Jia Z, Zheng J, Zeng C, Li L, *et al*. Rhein improves renal lesion and ameliorates dyslipidemia in db/db mice with diabetic nephropathy. Planta Medica. 2010; 76: 27–33.

[21] Xiong ZH. Effect of rhubarb on lipid and TGF-β1 level in patients with diabetic nephropathy. Journal of Hainan Medical University. 2012; 8: 1066–1068.

[22] Chen Y, Mu L, Xing L, Li S, Fu S. Rhein alleviates renal interstitial fibrosis by inhibiting tubular cell apoptosis in rats. Biological Research. 2019; 52: 50.

[23] Robins R, Baldwin C, Aoudjit L, Côté J, Gupta IR, Takano T. Rac1 activation in podocytes induces the spectrum of nephrotic syndrome. Kidney International. 2017; 92: 349–364.

[24] Lv Z, Hu M, Fan M, Li X, Lin J, Zhen J, *et al*. Podocyte-specific Rac1 deficiency ameliorates podocyte damage and proteinuria in STZ-induced diabetic nephropathy in mice. Cell Death & Disease. 2018; 9: 342.

[25] Lv Z, Hu M, Zhen J, Lin J, Wang Q, Wang R. Rac1/PAK1 signaling promotes epithelial-mesenchymal transition of podocytes in vitro via triggering β-catenin transcriptional activity under high

glucose conditions. The International Journal of Biochemistry & Cell Biology. 2013; 45: 255–264.
[26] Wu Y, Zhao Y, Yang H, Wang Y, Chen Y. HMGB1 regulates ferroptosis through Nrf2 pathway in mesangial cells in response to high glucose. Bioscience Reports. 2021; 41: BSR20202924.
[27] Wang X, Wu T, Ma H, Huang X, Huang K, Ye C, *et al*. VX-765 ameliorates inflammation and extracellular matrix accumulation by inhibiting the NOX1/ROS/NF-κB pathway in diabetic nephropathy. The Journal of Pharmacy and Pharmacology. 2022; 74: 377–386.
[28] Cheng G, Diebold BA, Hughes Y, Lambeth JD. Nox1-dependent reactive oxygen generation is regulated by Rac1. The Journal of Biological Chemistry. 2006; 281: 17718–17726.
[29] Duan S, Wu Y, Zhao C, Chen M, Yuan Y, Xing C, *et al*. The wnt/β-catenin signaling pathway participates in rhein ameliorating kidney injury in DN mice. Molecular and Cellular Biochemistry. 2016; 411: 73–82.
[30] Ferri N, Corsini A, Bottino P, Clerici F, Contini A. Virtual screening approach for the identification of new Rac1 inhibitors. Journal of Medicinal Chemistry. 2009; 52: 4087–4090.
[31] Su Z, Tian W, Li J, Wang C, Pan Z, Li D, *et al*. Biological evaluation and molecular docking of Rhein as a multi-targeted radiotherapy sensitization agent of nasopharyngeal carcinoma. Journal of Molecular Structure. 2017; 1147: 462–468.
[32] Wang L, Li H. MiR-770-5p facilitates podocyte apoptosis and inflammation in diabetic nephropathy by targeting TIMP3. Bioscience Reports. 2020; 40: BSR20193653.
[33] Fan H, Zhang W. Overexpression of Linc 4930556M19Rik Suppresses High Glucose-Triggered Podocyte Apoptosis, Fibrosis and Inflammation via the miR-27a-3p/Metalloproteinase 3 (TIMP3) Axis in Diabetic Nephropathy. Medical Science Monitor. 2020; 26: e925361.
[34] Zhang Q, Hu Y, Hu J, Ding Y, Shen Y, Xu H, *et al*. Sp1-mediated upregulation of Prdx6 expression prevents podocyte injury in diabetic nephropathy via mitigation of oxidative stress and ferroptosis. Life Sciences. 2021; 278: 119529.
[35] Zhang Q, Liu L, Lin W, Yin S, Duan A, Liu Z, *et al*. Rhein reverses Klotho repression via promoter demethylation and protects against kidney and bone injuries in mice with chronic kidney disease. Kidney International. 2017; 91: 144–156.
[36] Stockwell BR, Friedmann Angeli JP, Bayir H, Bush AI, Conrad M, Dixon SJ, *et al*. Ferroptosis: A Regulated Cell Death Nexus Linking Metabolism, Redox Biology, and Disease. Cell. 2017; 171: 273–285.
[37] Sagoo MK, Gnudi L. Diabetic nephropathy: Is there a role for oxidative stress? Free Radical Biology & Medicine. 2018; 116: 50–63.
[38] Zhong X, Huang G, Luo T, Deng Z, Hu J. Protective effect of rhein against oxidative stress-related endothelial cell injury. Molecular Medicine Reports. 2012; 5: 1261–1266.
[39] Bersuker K, Hendricks JM, Li Z, Magtanong L, Ford B, Tang PH, *et al*. The CoQ oxidoreductase FSP1 acts parallel to GPX4 to inhibit ferroptosis. Nature. 2019; 575: 688–692.
[40] Liu T, Cui Y, Dong S, Kong X, Xu X, Wang Y, *et al*. Treadmill Training Reduces Cerebral Ischemia-Reperfusion Injury by Inhibiting Ferroptosis through Activation of SLC7A11/GPX4. Oxidative Medicine and Cellular Longevity. 2022; 2022: 8693664.
[41] Feng H, Schorpp K, Jin J, Yozwiak CE, Hoffstrom BG, Decker AM, *et al*. Transferrin Receptor Is a Specific Ferroptosis Marker. Cell Reports. 2020; 30: 3411–3423.e7.
[42] Wang Y, Zhang M, Bi R, Su Y, Quan F, Lin Y, *et al*. ACSL4 deficiency confers protection against ferroptosis-mediated acute kidney injury. Redox Biology. 2022; 51: 102262.
[43] Xu Y, Ouyang C, Lyu D, Lin Z, Zheng W, Xiao F, *et al*. Diabetic nephropathy execrates epithelial-to-mesenchymal transition (EMT) via miR-2467-3p/Twist1 pathway. Biomedicine & Pharmacotherapy. 2020; 125: 109920.
[44] Hwang I, Uddin MJ, Lee G, Jiang S, Pak ES, Ha H. Peroxiredoxin 3 deficiency accelerates chronic kidney injury in mice through interactions between macrophages and tubular epithelial cells. Free Radical Biology & Medicine. 2019; 131: 162–172.
[45] Boini KM, Xia M, Xiong J, Li C, Payne LP, Li P. Implication of CD38 gene in podocyte epithelial-to-mesenchymal transition and glomerular sclerosis. Journal of Cellular and Molecular Medicine. 2012; 16: 1674–1685.
[46] Li Y, Kang YS, Dai C, Kiss LP, Wen X, Liu Y. Epithelial-to-mesenchymal transition is a potential pathway leading to podocyte dysfunction and proteinuria. The American Journal of Pathology. 2008; 172: 299–308.
[47] Bai X, Geng J, Zhou Z, Tian J, Li X. MicroRNA-130b improves renal tubulointerstitial fibrosis via repression of Snail-induced epithelial-mesenchymal transition in diabetic nephropathy. Scientific Reports. 2016; 6: 20475.
[48] Gao F, Li R, Wei P, Ou L, Li M, Bai Y, *et al*. Synergistic anticancer effects of everolimus (RAD001) and Rhein on gastric cancer cells via phosphoinositide-3-kinase (PI3K)/protein kinase B (AKT)/mammalian target of rapamycin (mTOR) pathway. Bioengineered. 2022; 13: 6332–6342.
[49] Marei H, Malliri A. Rac1 in human diseases: The therapeutic potential of targeting Rac1 signaling regulatory mechanisms. Small GTPases. 2017; 8: 139–163.
[50] Attias O, Jiang R, Aoudjit L, Kawachi H, Takano T. Rac1 contributes to actin organization in glomerular podocytes. Nephron. Experimental Nephrology. 2010; 114: e93–e106.
[51] Patel A, MacMahon S, Chalmers J, Neal B, Billot L, Woodward M, *et al*. Intensive blood glucose control and vascular outcomes in patients with type 2 diabetes. The New England Journal of Medicine. 2008; 358: 2560–2572.
[52] Remuzzi A, Perico N, Amuchastegui CS, Malanchini B, Mazerska M, Battaglia C, *et al*. Short- and long-term effect of angiotensin II receptor blockade in rats with experimental diabetes. Journal of the American Society of Nephrology. 1993; 4: 40–49.
[53] Jeong BY, Uddin MJ, Park JH, Lee JH, Lee HB, Miyata T, *et al*. Novel Plasminogen Activator Inhibitor-1 Inhibitors Prevent Diabetic Kidney Injury in a Mouse Model. PLoS ONE. 2016; 11: e0157012.
[54] Kanwar YS, Sun L, Xie P, Liu F, Chen S. A glimpse of various pathogenetic mechanisms of diabetic nephropathy. Annual Review of Pathology. 2011; 6: 395–423.
[55] Tu Y, Gu L, Chen D, Wu W, Liu H, Hu H, *et al*. Rhein Inhibits Autophagy in Rat Renal Tubular Cells by Regulation of AMPK/mTOR Signaling. Scientific Reports. 2017; 7: 43790.